J Therm Anal Calorim (2012) 109:1423–1427
DOI 10.1007/s10973-011-1829-6

Thermal degradation of a molecular magnetic material: $\{N(n\text{-}C_4H_9)_4[Fe^{II}Fe^{III}(C_2O_4)_3]\}_\infty$

A. Bhattacharjee · D. Roy · M. Roy

Received: 8 June 2011 / Accepted: 27 July 2011 / Published online: 13 August 2011

Abstract Thermal degradation of a mixed-valence oxalate based molecular material $\{N(n\text{-}C_4H_9)_4[Fe^{II}Fe^{III}(C_2O_4)_3]\}_\infty$ was investigated by thermogravimetric (TG) analysis. Considering the mass loss at each step of TG profile, possible step-wise thermal degradation reaction pathways of the precursor material are proposed which indicate the formation of hematite and magnetite as the solid end product of the degradation reaction. The IR spectroscopy and powder X-ray diffraction (XRD) studies of the thermally degraded samples supplement the proposed reaction pathways.

Keywords Thermal degradation · Molecular material · Oxalates

Introduction

The mechanism of a solid-state reaction, which is a collection of reaction steps, explains in detail as to how the overall reaction proceeds, and describes what takes place at each step of a solid-state chemical transformation. From the analysis of the experimental results of a thermal degradation, one can construct a reaction kinetic model of the chemical processes leading from the precursor(s) to the product(s) of a reaction [1]. One well-known ligand—oxalate can be coordinated with many transition and nontransition metals. Thermal degradation of the oxalate-based complexes is usually complicated and proceeds stepwise through a series of intermediate reactions involving the degradation of one phase and the formation of new one [2, 3]. Polymeric bimetallic oxalate complexes of general formula $\{A[M^{II}M^{III}(C_2O_4)_3]\}_\infty$, (A: organic cation, M^{II}, M^{III}: di-/trivalent transition metal ions; C_2O_4: oxalate ligand) have long been an important topic in the research of molecular magnetism due to the formation of quasi-2D layers of hexagonal oxalate-based magnetic networks [4–7]. Besides magnetic properties, thermal degradation of one such molecular ferromagnetic material $\{N(n\text{-}C_4H_9)_4[Mn^{II}Cr^{III}(C_2O_4)_3]\}_\infty$ has resulted into a spinel oxide—$Mn_{1.5}Cr_{1.5}O_4$ at $\sim$ 500 °C [8]. Recently, thermal degradation of one analogous molecular ferrimagnetic material $\{N(n\text{-}C_4H_9)_4[Fe^{II}Fe^{III}(C_2O_4)_3]\}_\infty$ has been reported to lead to the formation of ferrite (mainly, hematite) particles of mean crystallite size of 169 nm by the present authors [9]. These observations suggest that the molecular magnetic materials might be suitable for single-molecular precursors leading to various metal oxides.

In the present work, we study the thermal degradation of a molecular magnetic precursor $\{N(n\text{-}C_4H_9)_4[Fe^{II}Fe^{III}(C_2O_4)_3]\}_\infty$ (Scheme 1) and attempt to identify the reaction processes.

Experimental

The precursor material $\{N(n\text{-}C_4H_9)_4[Fe^{II}Fe^{III}(C_2O_4)_3]\}_\infty$ was prepared in one pot reaction according to the procedure reported earlier [4]. The powdery deep green colored sample thus obtained was used for the thermogravimetric (TG) study. The TG measurements were carried out using a thermogravimetric analyzer (TGA) of Netzsch, Germany

A. Bhattacharjee (✉) · D. Roy
Department of Physics, Visva-Bharati University, Santiniketan, India
e-mail: ashis.bhattacharjee@visva-bharati.ac.in

M. Roy
Applied Material Science Division, Saha Institute of Nuclear Physics, Kolkata, India

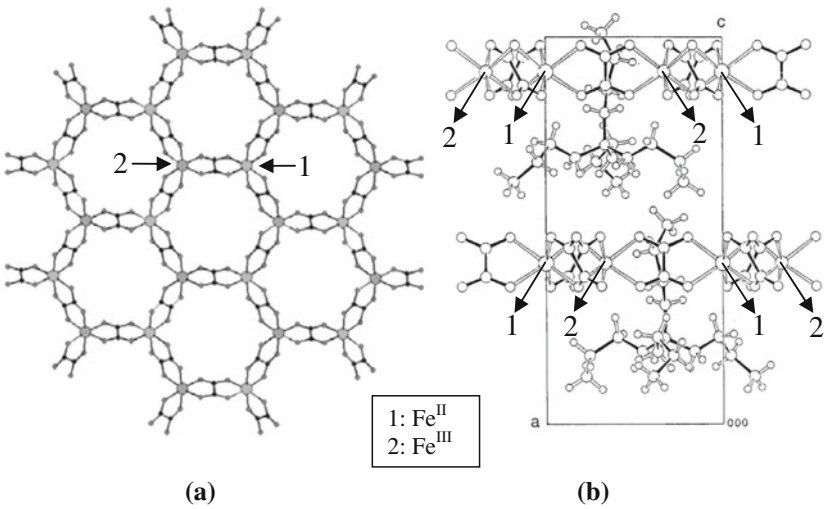

Scheme 1 Schematic projections: **a** infinitely extended [–Fe^{II}–oxalate–Fe^{III}–] layer; the tetra-*n*-butyl ammonium cation, [N(*n*-$C_4H_9)_4]^+$ is not shown, and **b** {N(*n*-$C_4H_9)_4[Fe^{II}Fe^{III}(C_2O_4)_3]\}_\infty$ with $[N(n\text{-}C_4H_9)_4]^+$ cation interleaved within the interlayer space (adopted from [5])

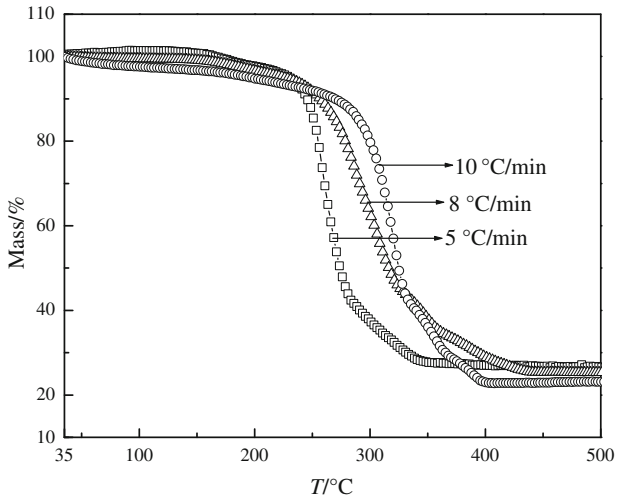

Fig. 1 TG profiles of $\{N(n\text{-}C_4H_9)_4[Fe^{II}Fe^{III}(C_2O_4)_3]\}_\infty$ at different heating rates

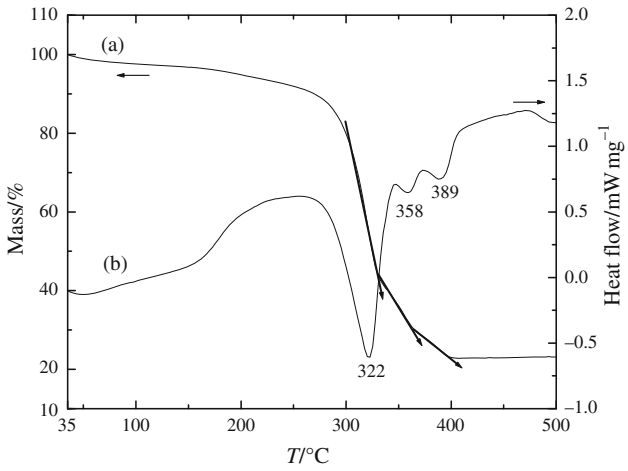

Fig. 2 *a* TG profile and *b* DSC profile of $\{N(n\text{-}C_4H_9)_4[Fe^{II}Fe^{III}(C_2O_4)_3]\}_\infty$ obtained at 10 °C/min heating rate exhibiting the different temperature ranges (step-I, step-II, and step-III) of thermal degradation

(model: STA 449C). IR spectra were recorded with Shimadzu made spectrophotometer (model: 8400S), whereas the powder XRD scans were obtained with XRD (Phillips).

Results and discussion

The thermal degradation of $\{N(n\text{-}C_4H_9)_4[Fe^{II}Fe^{III}(C_2O_4)_3]\}_\infty$, say Fep1, was monitored by TGA at three different heating rates (5, 8, and 10 °C/min). The TG curves thus obtained are shown in Fig. 1. The degradation proceeds through few intermediate phases, and finally results into the formation of a powdery deep red product. Comparison of the TG profiles obtained at different heating rates indicates that the use of higher heating rate helps to resolve the presence of intermediate phases, which is not clearly seen when the sample is heated at lower heating rate. However, this trend is just opposite to that observed in the case of thermal degradation of epsomite crystals in the presence of organic additives [10].

Figure 2 shows the TG and DSC profiles of Fep1, obtained at 10 °C/min heating rate along with different steps of thermal degradation. From this figure, it is seen that a very gradual mass loss sets in at ~43 °C and continues till ~280 °C where the mass loss is recorded to be ~12%. As no phase transition is indicated in the DSC result, this loss of mass may be attributed to the loss of adsorbed moisture. At this point, it should be noted that Fep1 has no crystalline water associated with. Beyond 280 °C, the thermal degradation proceeds with rapid mass loss through three linear steps, indicating different stages of solid state reaction of Fep1. These three linear steps are indicated by arrows which fall in the temperature ranges:

(i) 283–333 °C, (ii) 333–365 °C, and (iii) 365–400 °C, mentioned as step-I, step-II, and step-III, respectively. Thus, Fep1 undergoes successive solid-state reactions in these three steps. The mass loss values estimated at the completion of step-I, step-II, and step-III of thermal degradations are ~45, ~12.4, and ~7%, respectively. Thermal degradation becomes complete at ~400 °C and no further change in mass is recorded in the TG profile above 400 °C up to 630 °C. It is to be noted that at 5 °C/min heating rate the step-II and step-III are merged into a single step. The result obtained from simultaneous DSC study is shown in Fig. 2 (plot b). The endothermic DSC peaks appear at ~322, ~358, and ~389 °C which fall within the step-I, step-II and step-III, respectively, of the TG curve, confirming the three solid-state reactions and the corresponding phase transitions.

A solid-state reaction involves the breaking and formation of chemical bond(s) through single or multiple steps. In an attempt to know the nature of the degraded material at the ends of different steps of TG and thereby to understand the step-wise thermal degradation reaction process, IR and XRD studies of the degraded materials have been carried out.

To carry out IR studies of the degraded products at different stages of the thermal degradation reaction, two samples were prepared keeping the precursor material inside a furnace, initially with air ambient, at temperatures 330 ± 5 and 360 ± 5 °C, which are very close to the end temperatures of step-I and step-II, respectively. The IR spectra obtained for these samples (say, S_I and S_{II}) are shown in Fig. 3. In the IR spectra for S_I (Fig. 3 (plot a)), there are absorption bands at ~460 and, ~545, ~620, and ~1,635 cm^{-1}. The first three observed bands indicate the presence of metal–oxygen bonds in general, and the existence of hematite in the sample S_I [11, 12] in particular. The presence of the band at ~1,635 cm^{-1} corresponds to C=O stretching vibration and indicates the presence of oxalate bonds in the material at this temperature. This implies that at this stage not all of the oxalate ligands are decomposed. In the IR spectrum of S_{II} (Fig. 3 plot b), the absorption band at ~460 cm^{-1} confirms the existence/formation of hematites at this temperature range. In addition to this band, another band at ~580 cm^{-1} in the IR spectrum of S_{II} appears which corresponds to magnetite. The appearance of a weak C=O bond is also noted, though incompleteness of the thermal degradation of the oxalate bonds at this temperature is unlikely. This might have occurred due to instrumental error. The IR spectra of the completely degraded sample (after step-III), reported previously by the present authors, showed several distinct bands in support of unequivocal presence of hematite in the final degraded product [9]. The presence of both hematite and magnetite in the final degraded product was also confirmed through magnetization studies [9].

Figure 4 (plot a) shows the powder XRD scan of Fep1 before the start of thermal degradation, whereas Fig. 4 (plot b) illustrates the powder XRD scan of the sample obtained on thermal degradation of the precursor inside the TG instrument at 370 °C. This temperature is also close to the end temperature of step-II as evident from the TG profile. It is noticed that the main peaks corresponding to the precursor Fep1 (see Fig. 4 (plot a)) are retained in Fig. 4 (plot b) though some new peaks appear. On comparison of Fig. 4 (plot a) with Fig. 4 (plot b), it is clearly observed that the precursor material has apparently been completely degraded. The sharp peaks, observed in Fig. 4

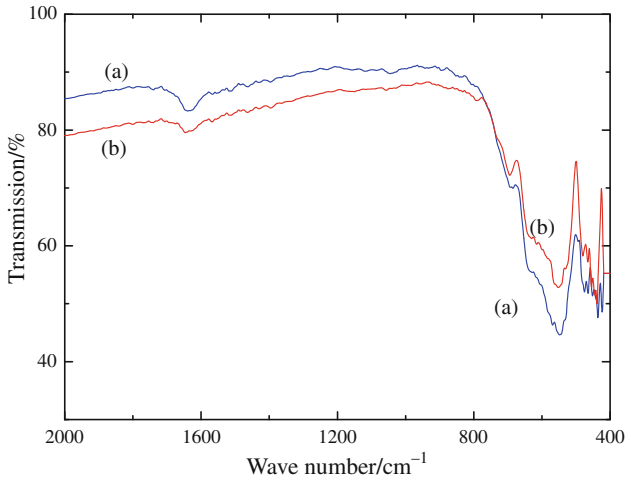

Fig. 3 IR spectra of *a* S_I (obtained after keeping $\{N(n\text{-}C_4H_9)_4[Fe^{II}Fe^{III}(C_2O_4)_3]\}_\infty$ in a furnace at 330 ± 5 °C for 4 h, and *b* S_{II} (obtained after keeping $\{N(n\text{-}C_4H_9)_4[Fe^{II}Fe^{III}(C_2O_4)_3]\}_\infty$ in a furnace at 360 ± 5 °C for 4 h)

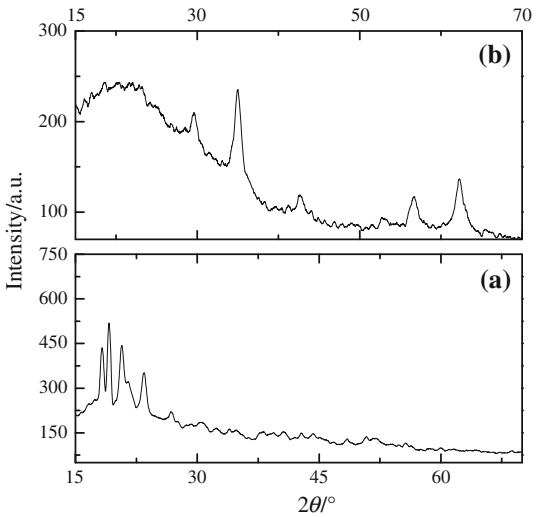

Fig. 4 XRD scans of $\{N(n\text{-}C_4H_9)_4[Fe^{II}Fe^{III}(C_2O_4)_3]\}_\infty$: **a** Before thermal degradation, **b** After thermal degradation up to 370 °C

(plot b), correspond to hematites [9]. Thus, the precursor—Fep1 at this stage of thermal degradation produces hematite. Additionally, magnetite may be present at this stage which perhaps could not be detectable in the spectra with the present statistically low quality XRD data [9].

Thus, the powder XRD results supplement the observations made through the IR studies. To understand the differences between the IR and XRD spectra, it has to be noted that the sample environment during thermal degradation inside the TG instrument and that inside the furnace were different. Moreover, it has to be noted that the temperature ranges of step-II and step-III are very narrow in comparison to that of step-I, as a result of which it may be practically difficult to control the temperature at the adjoining region of the step-II and step-III. This will also lead to practical difficulty in producing and identifying the products out of these steps in a furnace.

Considering the experimental results and mass loss values during the degradation step(s), an attempt to predict the reaction pathway(s) as well as the reaction product(s) at the end of the successive reaction step(s) of the thermal degradation is made. The thermal degradation process of $\{N(n\text{-}C_4H_9)_4[Fe^{II}Fe^{III}(C_2O_4)_3]\}_\infty$ may be proposed as follows:

Step-I:

$$2\{N(n-C_4H_9)_4[Fe^{II}Fe^{III}(C_2O_4)_3]\}_\infty \rightarrow [Fe^{II}Fe^{III}(C_2O_4)_{3-x}] + Fe_2O_3(s) + 2(n-C_4H_9)_3N(g) + 2C_4H_8(g) + (3+2x)CO_2(g) + 3CO(g) + H_2(g)$$

Step-II and step-III:

$$6[Fe^{II}Fe^{III}(C_2O_4)_{3-x}] \rightarrow 3Fe_2O_3(s) + 2Fe_3O_4(s) + (19-12x)CO_2(g) + 17CO(g)$$

where "g" and "s" denote gaseous and solid substances, respectively, and x is a positive number (<3). The observed mass loss values are well compared with the calculated mass loss values following the reaction pathways. Thus, the proposed reaction pathways indicate the formation of either Fe_3O_4 (magnetite) or Fe_2O_3 (hematite) or a mixture of both as a result of degradation of the precursor which has been supplemented by the present IR and XRD studies and confirmed by earlier magnetic studies [9]. Thermal degradation of iron oxalate to hematite in air atmosphere and to magnetite in presence of CO/CO_2 mixture are reported by other workers [13]. In the present case, inside the furnace the thermal degradation initially started in air atmosphere leading to the formation of hematite along with profuse amount of CO_2 and subsequently, on further heating it might have led to the formation of magnetite [14]. Formation of trace amount of maghemite during this thermal degradation process, though could not be detected, may not be ruled out.

Conclusions

In the present study, thermal degradation of a bimetallic oxalate ligand based molecular magnetic material $\{N(n\text{-}C_4H_9)_4[Fe^{II}Fe^{III}(C_2O_4)_3]\}_\infty$ was investigated by TG analysis. Taking the solid state reaction processes of the material of interest are of multi steps, the chemical products and reaction pathways are established using TG measurement and supplemented by the IR and powder XRD studies. The thermal degradation reaction in the present case results into the formation of hematite and magnetite. This work could provide a methodology to prepare hematite and/or magnetite from suitable molecular precursors under controlled thermal degradation. Furthermore, it may generally invoke interest to prepare different metal oxides of interest under controlled thermal degradation and to study kinetics of the solid-state reaction to identify the rate controlling process for better synthesis and maneuvering.

References

1. Yang HC, Eun HC, Cho YZ, Lee HS, Kim IT. Kinetic analysis of dechlorination and oxidation of PrOCl by using a non-isothermal TG method. Thermochim Acta. 2009;484:77–81.
2. Brown ME. Introduction to thermal analysis techniques and applications. 2nd ed. Dordrecht: Kluwer Academic Publishers; 2004.
3. Donkova B, Kotzeva B, Vasileva P, Mehandjiev D. Thermal magnetic investigation of the decomposition of $Ni_xMn_{1-x}C_2O_4{\cdot}2H_2O$. Thermochim Acta. 2009;481:12–9.
4. Ōkawa H, Matsumoto N, Tamaki H, Kida S, Ohba M. Ferrimagnetic mixed-metal assembles $\{NBu_4\ [MFe(ox)_3]\}_x$. Mol Cryst Liq Cryst. 1993;233:257–62.
5. Pellaux R, Schmalle HW, Huber R, Fischer P, Hauss T, Ouladdiaf B, 'Decurtins S. Molecular-based magnetism in bimetallic two-dimensional oxalate bridged networks. An X-ray and neutron diffraction study. Inorg Chem. 1997;36:2301–8.
6. Bhattacharjee A, Reiman S, Ksenofontov V, Gütlich, P. Mössbauer spectroscopy under a magnetic field to explore the low-temperature spin structure of the layered ferromagnetic material—$\{N(n\text{-}C_4H_9)_4[Fe^{II}Fe^{III}(C_2O_4)_3]\}_\infty$. J Phys Condens Matter. 2003;15:5103–12.
7. Bhattacharjee A, Balanda M, Miyazaki Y, Sorai M, Gütlich P. Uncompensated magnetization in the layered molecular antiferromagnet $\{N(n\text{-}C_5H_{11})_4[Mn^{II}Fe^{III}(ox)_3]\}_\infty$. Polyhedron. 2009;28:2899–904.
8. Neo KE, Ong YY, Huynh HV, Andy Hor TS. A single-molecular pathway from heterometallic MM' ($M = Ba^{II}, Mn^{II}$; $M' = Cr^{III}$) oxalato complexes to intermetallic composite oxides. J Mater Chem. 2007;17:1002–6.
9. Bhattacharjee A, Roy D, Roy M, Chakraborty S, De A, Kusz J, Hofmeister W. Rod-like ferrites through thermal degradation of a molecular ferrimagnet. J Alloy Compd. 2010;503:449–53.
10. Ruiz-Agudo E, Martin-Ramos JD, Rodriguez-Navarro C. Mechanism and kinetics of dehydration of epsomite crystals formed in the presence of organic additives. J Phys Chem B. 2007;111:41–52.

11. Gillot B. Infrared spectrometric investigation of submicron metastable cation-deficient spinels in relation to order-disorder phenomena and phase transition. Vib Spectrosc. 1994;6:127–48.
12. Kustova GN, Burgina EB, Sadykov VA, Poryvaev SG. Vibrational spectroscopic investigation of the goethite thermal decomposition products. Phys Chem Miner. 1992;18:379–82.
13. Angermann A, Töffer J. Synthesis of magnetite nanoparticles by thermal decomposition of ferrous oxalate dehydrate. J Mater Sci. 2008;43:5123–30.
14. Lyubutin IS, Lin CR, Korzhetskiy Yu V, Dmitrieva TV, Chiang RK. Mössbauer spectroscopy and magnetic properties of hematite/magnetite nanocomposites. J Appl Phys. 2009;106:34311–6.